University of Nebraska UAS profiling during LAPSE-RATE

Ashraful Islam[1], Ajay Shankar[1], Adam Houston[2], and Carrick Detweiler[1]

[1]NIMBUS Lab, Department of Computer Science & Engineering, University of Nebraska-Lincoln, Lincoln, NE 68588, USA.
[2]Department of Earth & Atmospheric Sciences, University of Nebraska-Lincoln, Lincoln, NE 68588, USA.

Correspondence: Ashraful Islam (mislam@huskers.unl.edu)

Abstract.

This paper describes the data collected by the University of Nebraska-Lincoln (UNL) as part of the field ~~deployment~~ deployments during the Lower Atmospheric Process Studies at Elevation — a Remotely-piloted Aircraft Team Experiment (LAPSE-RATE) flight campaign in July 2018. UNL deployed two multirotor unmanned aerial systems (UASs) at ~~various~~ multiple sites in the San Luis Valley (Colorado, USA) for data collection ~~in support of~~ to support three science missions: convection-initiation, boundary layer transition, and cold air drainage flow. We conducted 172 flights resulting in over ~~1300 minutes~~ 21 hours of cumulative flight time. Our novel design for the sensor housing onboard the UAS was employed in these flights to meet the aspiration and shielding requirements of the temperature ~~/humidity sensors , and attempt~~ and humidity sensors and to separate them from the mixed turbulent airflow from the propellers. Data presented in this paper include ~~time-stamped~~ timestamped temperature and humidity data collected from the sensors, along with the three-dimensional position and velocity of the UAS. Data are quality controlled and time-synchronized using a zero-order-hold interpolation without additional ~~post processing~~post-processing. The full dataset is also made available for download at (https://doi.org/10.5281/zenodo.4306086 (Islam et al., 2020)).

1 Introduction

A team of researchers from the University of Nebraska-Lincoln (UNL) participated in the Lower Atmospheric Process Studies at Elevation —- a Remotely piloted Aircraft Team Experiment (LAPSE-RATE) flight campaign between 14 – 19 July 2018 at San Luis Valley of Colorado, USA. LAPSE-RATE was organized as part of the International Society for Atmospheric Research using Remotely piloted Aircraft (ISARRA) 2018 meeting. A total of 1287 flights were conducted by 13 institutions, including UNL, which resulted in more than 260 hours of data collection. UNL's contribution to this collaborative data collection effort was 172 Atmospheric Boundary Layer (ABL) profiling flights using two multirotor UAS platforms. These flights from UNL resulted in over 21 hours of data being collected. This unique collaboration resulted in a collective sampling of a variety of atmospheric phenomena over the span of six days at preplanned sites around the San Luis Valley. An overview of the LAPSE-RATE campaign, the description of site locations, and science missions that focused on measuring different atmospheric phenomena of interest are documented (de Boer et al., 2020a, b). Data from UNL and all other participating teams in the LAPSE-RATE campaign are hosted in an open access data repository (LAPSE-RATE Data Repository, 2021).

Multirotor UASs are finding more routine uses for sampling and profiling the ~~atmospheric boundary layer (ABL) (Elston et al., 2015; Bo~~ ~~UASs enable such profiling~~ ABL, such as atmospheric profiling (Bonin et al., 2013; Elston et al., 2015; Greatwood et al., 2017; Jacob et al. estimation of the spatial structure of temperature (Hemingway et al., 2020), wind measurement (Prudden et al., 2016; Palomaki et al., 2017 and prediction of Lagrangian coherent structure (Nolan et al., 2018).

The need for increased spatial resolution for atmospheric sampling is reflected in publications, such as improving Numerical Weather Prediction (NWP) models (Leuenberger et al., 2020), improvement of mesoscale atmospheric forecast (Dabberdt et al., 2005), and identification of hazardous weather for Beyond Visual Line of Sight(BVLOS) flights using UAS Traffic Management (UTM) systems (Mitchell et al., 2020). UASs can meet such profiling needs with a greater frequency ~~, increased spatio-temporal~~ of profiles, increased spatiotemporal resolution of data, and sampling in virtually any sampling location when compared with traditional methods. Multirotors extend ~~this~~ the sampling capability by allowing rapid and repeatable ~~fixed-site profiling .~~ profiling at any site while maintaining a fixed horizontal position.

Our previous work (Islam et al., 2019) describes the design and evaluation of a ~~temperature-humidity~~ temperature and humidity (TH) sensor housing that meets the recommended sensor placement, aspiration, and shielding criteria by using a passively induced-airflow technique that works by exploiting the existing UAS propeller. The housing's inlet is pointed outwards from the UAS to sample just outside of the UAS turbulence in both ascent and descent. This is different from existing methods of placing the sensor under the arm without shielding but aspirated by the propeller (Hemingway et al., 2017), on the body of the UAS without shielding and aspiration (Lee et al., 2018), on a different part of the UAS with shielding and possible aspiration from propellers (Greene et al., 2018) or shielding the sensor inside UAS and active aspiration using a fan while pointing the inlet towards the wind (Greene et al., 2019). All of these existing configurations fail to produce reliable data during descent, and these data are usually discarded (Lee et al., 2018). As multirotor flight time is very limited, needing to discard entire descent data prevents optimal use of resources. Additionally, in most cases, observations are affected by wind direction and require onboard sensing of wind and reorientation of UAS with the change of wind direction (Greene et al., 2019). ~~The sensor housingdesign has evolved over multiple design iterations and has been field tested in multiple CLOUD-MAP field campaigns (Jacob et al., 2018; ?).~~

Two primary highlights of ~~the~~ our novel sensor housing are ~~the ability to reliably obtain sensor reading~~ its ability to obtain temperature and humidity sensor readings reliably during both ascent and descent profiles, and its invariance to the aircraft orientation relative to the ambient wind. Two key design considerations ~~to achieve~~ in achieving these goals are: the placement of the sensor~~and~~ , and its consistent aspiration. Placement of the sensor on the UAS body can adversely affect the measurements (Greene et al., 2018; Jacob et al., 2018). ~~According to experimental resultspresented by~~As observed through prior experimental results (Villa et al., 2016), the ~~validity of the measurement increases farther away~~ accuracy of a sensor's measurement increases the farther away it is placed from the propeller's downwash. More specifically~~from (Prudden et al., 2016), sensors placed at least 2.5×~~ , a sensor placed at a distance at least 2.5 times the propeller diameter away from the rotor experiences significantly less ~~propeller interference~~aerodynamic interference (Prudden et al., 2016). Consistent and sufficient aspiration is also necessary for a consistent effective sensor response time (Houston and Keeler, 2018). Placing the sensor inside the propeller region or near the body can result in inconsistent aspiration due to rotor turbulence ~~(?Yoon et al., 2017)~~(Diaz and Yoon, 2018; Yoo

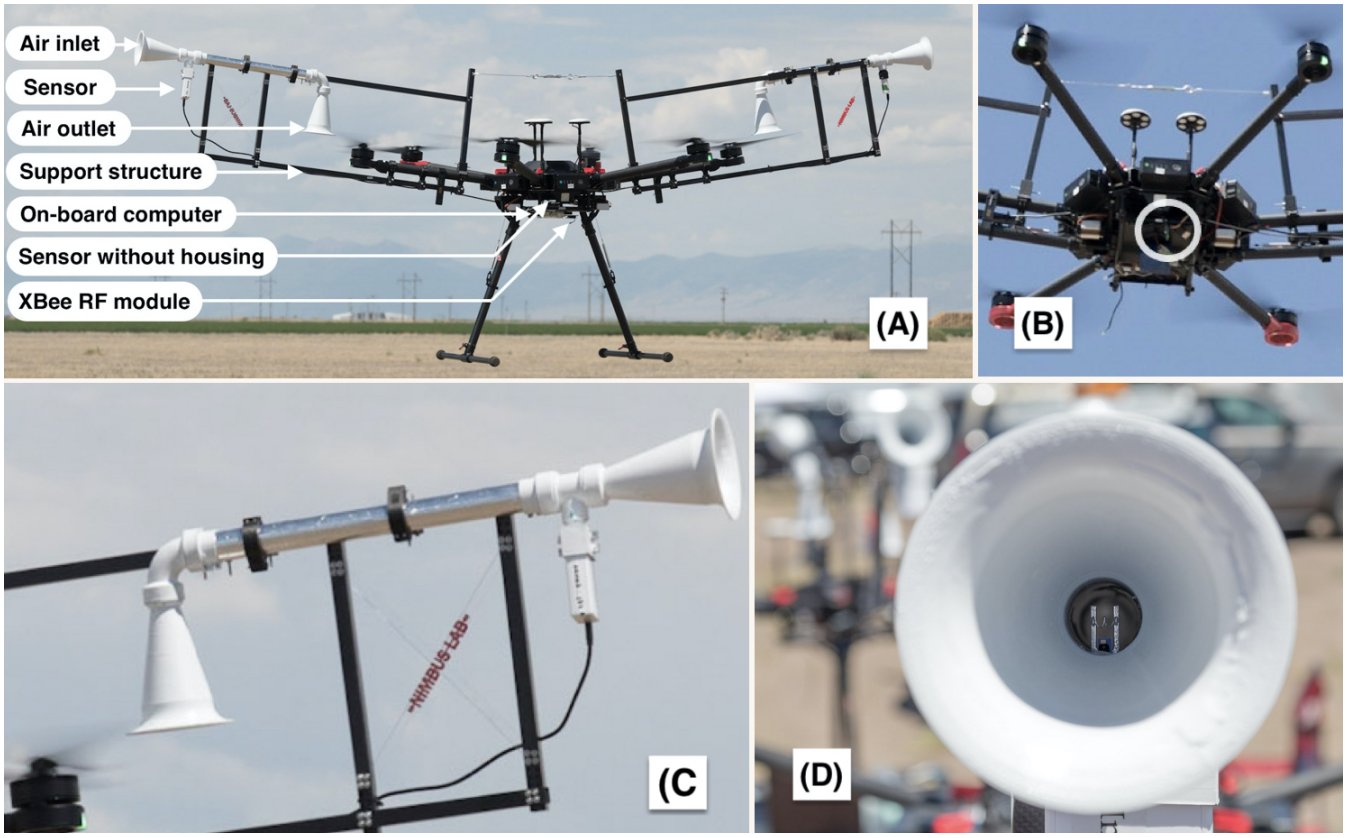

Figure 1. Images of (A) the UAS setup with the temperature and humidity sensor mounted in the aspirated and shielded sensor housing, and in a traditional configuration (B) Close up of the traditionally mounted sensor under the UAS without the sensor housing (inside the white circle), (C) Close up of the sensor housing with the sensor mounted, and (D) Close up of the sensor probe mounted inside our sensor housing. The outlet of the sensor housing is placed on top of the propeller, and the inlet is pointing outward. High-speed air in the sensor housing is drawn passively by exploiting the pressure deficit created by the propeller of the UAS.

As such, we designed our sensor housing to source the sampling air from outside rotor interference ~~,~~ and to maintain consistently high aspiration ~~air speed~~ airspeed to obtain reliable results. ~~Detailed~~

Our sensor housing design has evolved over multiple design iterations and has been field-tested in multiple Collaboration Leading Operational UAS Development for Meteorology and Atmospheric Physics (CLOUD-MAP) field campaigns (Jacob et al., 2018). The details of our data validations tests, as well as a complete description of the sensor housing design ~~along with the verification of data~~ , are available in ~~the~~ a separate open access paper (Islam et al., 2019).

For the LAPSE-RATE campaign, UNL deployed two identical UASs with one primary sensor suite for measurements, and a secondary sensor suite for redundancy and testing. These flights were conducted at five locations in San Luis Valley (Colorado, USA) through 14–19 July 2018. The maximum altitude for each flight ranged from $100 - 500\,\mathrm{m}$ above ground level. Figure 1 ~~shows a picture of~~ illustrates the UAS with the housing setup. ~~Both~~ , closeup of the sensor housing, and sensor

mounting configurations. Both primary and secondary sensors are located inside their respective sensor housings mounted on two diametrically opposing arms of the UAS. In some flights, a third sensor was mounted *under* the ~~body-center~~ body frame of the UAS to compare the performance of primary sensors against traditional mounting positions. A detailed description of our configuration is presented in Section 2.5. It should be noted that, although the data collection is focused on the temperature and humidity measurements, atmospheric pressure data from the sensors are also included in the dataset for anyone interested.

~~UNL deployed the UASs in five locations in San Luis Valley (Colorado, USA), through 15-19 July 2018. The maximum flight altitude for each flight ranged from 100 - 500 above ground level. We conducted 172 flights over a span of 4 days.~~ The rest of the paper describes the ~~systems, flight strategies, data processing and quality controls and sample of the data~~components of our system (Section 2), the flight strategies employed for missions (Section 3), the data processing used (Section 4), and some special topics of interest (Section 5). We finally conclude with an example profile data, and provide details regarding the availability of the dataset.

~~UAS setup with temperature-humidity sensor mounted in aspirated and shielded sensor housing.~~

2 System Description

2.1 UAS platform

The two identical UASs deployed during the missions were developed on a DJI Matrice 600Pro platform equipped with DJI A3 Pro flight control systems. ~~Unfolded~~ The unfolded dimensions (including propellers, frame arms, GPS mounts, and landing gear) of the system are ~~$1668mm \times 1518mm \times 727mm$~~$1668\,\mathrm{mm} \times 1518\,\mathrm{mm} \times 727\,\mathrm{mm}$. The recommended maximum payload capacity of the platform is ~~kg~~$5.5\,\mathrm{kg}$. At no load, the UAS has a flight endurance of ~~35–40 min~~ $35-40\,\mathrm{min}$ on a single set of six DJI TB48S batteries. The manufacturer-specified positioning accuracy is ~~±~~$\pm 0.5\,\mathrm{m}$ in the vertical axis, and ~~±mhorizontal (?)~~$\pm 1.5\,\mathrm{m}$ horizontal (DJI, 2021b). The maximum ascent and descent speeds are ~~m/sand m/s~~$5\,\mathrm{m\,s^{-1}}$ and $3\,\mathrm{m\,s^{-1}}$, respectively. The flight controller offers real-time access (read-only) to UAS's ~~on-board~~ onboard sensor data, such as position, velocity, and attitude, through a serial interface. Additionally, a mobile application allows a user to plan and deploy a flight trajectory, and the remote controller allows intervention from the user at any point.

2.2 Sensors~~:~~

~~Specifications of the temperature-humidity~~ Table 1 describes the specifications of the temperature and humidity (TH) sensors ~~recorded in the datasetare described in Table 1~~used for the dataset. Every UAS flight used one iMet XQ2 from InterMet Systems (Grand Rapids, MI, USA) as the primary TH sensor. The XQ2 is a self-contained sensor package designed for UASs to measure atmospheric pressure, temperature, and relative humidity. It is also equipped with a built-in GPS ~~,~~ and an internal data logger along with a rechargeable battery. A serial interface provides access to the logs, or real-time observations produced by the sensor at ~~1Hz~~1 Hz. The internal data-logger was only used as backup and is not part of this dataset. Data included in the

Table 1. The key manufacturer's specifications for the sensors used in different experiments: The unavailable fields are left blank. ~~Data sheet~~ Datasheet for each sensor packages are available at iMet XQ2 (InterMet Systems, 2021b), iMet XQ1 (InterMet Systems, 2021a), and nimbus-pth ~~(?)~~(Digikey, 2021; Mouser, 2021)

		XQ2 (iMet XQ2)	**XQ1 (iMet XQ1)**	nimbus-pth **(Custom Built)**
Temperature	Type	Bead Thermistor	Bead Thermistor	Bead Thermistor
	Range	-90 to $50\,^{\circ}\mathrm{C}$	-95 to $50\,^{\circ}\mathrm{C}$	-40 to $100\,^{\circ}\mathrm{C}$
	Response Time	$1\,\mathrm{s}$ @ $5\,\mathrm{m\,s^{-1}}$	$2\,\mathrm{s}$	
	Resolution	$0.01\,^{\circ}\mathrm{C}$	$0.01\,^{\circ}\mathrm{C}$	$0.01\,^{\circ}\mathrm{C}$
	Accuracy	$\pm 0.3\,^{\circ}\mathrm{C}$	$\pm 0.3\,^{\circ}\mathrm{C}$	
Humidity	Type	Capacitive	Capacitive	Capacitive
	Range	$0-100\,\%\,\mathrm{RH}$	$0-100\,\%\,\mathrm{RH}$	$0-100\,\%\,\mathrm{RH}$
	Response Time	@ $25\,^{\circ}\mathrm{C}$, $0.6\,\mathrm{s}$ @ $5\,^{\circ}\mathrm{C}$, $5.2\,\mathrm{s}$ @ $-10\,^{\circ}\mathrm{C}$, $10.9\,\mathrm{s}$	$5\,\mathrm{s}$ @ $1\,\mathrm{m\,s^{-1}}$ velocity	$8\,\mathrm{s}$
	Resolution	$0.1\,\%\,\mathrm{RH}$	$0.7\,\%\,\mathrm{RH}$	$0.01\,\%\,\mathrm{RH}$
	Accuracy	$\pm 5\,\%\,\mathrm{RH}$	$\pm 5\,\%\,\mathrm{RH}$	$\pm 2\,\%\,\mathrm{RH}$

dataset ~~are~~ were collected through the ~~DAQ~~ data acquisition (DAQ) system using the serial interface. Some UAS flights ~~feature~~ featured an older version of this sensor, called iMet XQ1, as the secondary backup sensor.

Some flights also ~~use a~~ used a nimbus-pth as the secondary sensor, which is a ~~pressure, temperature and humidity sensor~~ sensor package unit we designed and built ~~. Several can be stacked as nodes , and in~~ for pressure, temperature, and humidity sensors. Several nimbus-pth can be chained as nodes for data collection. In some data files~~two of them~~ , two of these nodes might be present. In such cases, one of them ~~is~~ was aspirated inside our sensor housing, and ~~other one sits~~ the other one sat directly underneath the UAS in a traditional non-aspirated configuration. In the data files, the first two sensors ~~are~~ were shielded and aspirated inside the housing, and the third sensor (when available) ~~is in~~ was in a traditional non-aspirated configuration.

2.3 Sensor Housing

The sensor housing is designed to meet or exceed sensor placement requirements, such as ~~constant~~ consistent aspiration for the sensors, shielding from ~~the~~ solar radiation and other indirect heat sources. The housing draws air passively by exploiting the pressure differential between the region just above a propeller and the region just beyond the rotor wash. The airflow through the housing is always maintained as long as the propellers are spinning, and provides a consistent aspiration for the sensors (Islam et al., 2019). The inlet and outlet of the housing are shaped ~~as~~ like a cone to provide ~~high speed~~ high-speed airflow across the housing tube with a small pressure difference between the two ends. Additional design considerations are

made to ensure that the flow is consistent, and provides airflow $\geq 5\,\mathrm{m\,s^{-1}}$ across the sensors even at the lowest propeller speeds.

~~The housing is~~ Sensors are placed inside the tube structure as shown in the panel C and D of Figure 1. The entire sensor housing is painted with reflective white paint, and tubes are wrapped with aluminum foil tape. This results in excellent rejection of solar heating and avoids unpredictable radiation heating bias. Such placement of sensors provides solar shielding and shielding from other artificial heat sources such as motor or battery waste heat. Since the entire housing is placed outside the body of UAS, it creates further isolation from the artificial heat sources in the UAS. Additionally, since the aspirating airspeed is very high (Islam et al., 2019), it reduces the error from all these sources even further (Anderson and Baumgartner, 1998).

The housing is also designed to be modular, printed entirely using a 3D printer, and has an easy screw-in assembly. ~~Impact~~ The impact of the housing on the UAS's stability and flight time is minimal. Further details and the full schematic of the housing and the evaluation can be found in our previous work (Islam et al., 2019).

2.4 Data acquisition~~:~~

Data ~~are~~ were collected using a data acquisition (DAQ) system ~~made of~~ comprised of an Odroid XU4 (Hardkernel, 2021), a compact single-board computer ~~, Odroid XU4 (?) running a linux~~ that runs a Linux operating system. Odroid runs the robot operating system (ROS) ~~(ROS, 2021)~~ (Quigley et al., 2009) that communicates with the serial devices through ~~the USB port of the Odroid~~its USB ports. ROS facilitates collecting many different sensor data independently at their own output frequency~~;~~, recording the timestamp for when data were generated and when they are received by ROS. ROS interfaces the collection of all available devices even in the case of a single device ~~fail~~failure. Synchronization of the data can either be done at runtime or in ~~the~~ post-processing. In our case, it ~~is done in the~~ was done in post-processing using MATLAB.

The communication with the DJI flight controller was implemented using the ROS interface of DJI Onboard SDK (DJI, 2021c) available to developers. This allowed the recording of all the telemetry data from the flight controller, along with high-quality positioning information. The GPS data from the iMet XQ2/ iMet XQ1 sensor were discarded as the positioning information from the flight controller was found to be of better quality.

The Odroid was connected with a ground computer using wireless ~~2.4 GHz~~ 2.4 GHz XBee radios for the operation of DAQ, debugging, and periodic checks on the data when the UAS finished a flight. The data collected by the DAQ were retrieved to the ground computer for archiving at the end of each day using an ethernet connection.

~~Temperature-humidity sensors connect~~ Temperature and humidity sensors were connected over serial with ROS to send periodic updates of the observations. The UAS's autopilot also ~~interface~~ interfaced with ROS to provide updates of position, velocity, altitude, attitude, etc. which ~~are~~ were also recorded to spatially and temporally synchronize the observation.

2.5 UAS Sensor Mounting Configuration and Payload~~:~~

As mentioned in ~~the subsection~~Subsection 2.2, the primary sensor ~~is the~~ was the iMet XQ2, and its data ~~are~~ were recorded on the dataset with a header underscore _1 (e.g., Temperature_1, Humidity_1, Pressure_1). Other sensor data headers ~~are~~ were followed with _2 and _3 when available. Sensor_1 and Sensor_2 ~~is~~ were shielded inside the sensor housing~~, however~~; however,

sensor_3 ~~is~~ was placed under the UAS in a traditional configuration without aspiration. ~~Specific~~ The placement of the sensors inside the housing and sensors without the housing are marked in Figure 1 for reference. Specific placements of the sensors on the UAS used in the data collection are described below.

~~**UAS platform M600P1**~~

2.5.1 UAS platform M600P1

One XQ2 (sensor_1) ~~is~~ was placed inside the left sensor housing, and one XQ1 (sensor_2) ~~is on a~~ was on an identical right sensor housing. This placement location for the left housing is highlighted in the 'panel (A)' of Figure 1. The alternative setup used in some experiments ~~replaces~~ replaced XQ1 with nimbus-pth (sensor_2) inside the right sensor housing (sensor names are also listed in metadata as data source). ~~An additional~~ If nimbus-pth ~~(sensor_3) is also~~ is included in measurements, it was placed under the body of the UAS without ~~housing whenever nimbus-pth is included in measurements~~any housing structure, as highlighted in the 'panel (A)' and 'panel (B)' of Figure 1.

~~**UAS platform M600P2**~~

2.5.2 UAS platform M600P2

One XQ2 (sensor_1) ~~is~~ was mounted inside the left sensor housing, one nimbus-pth (sensor_2) ~~is~~ was mounted inside the right sensor ~~sensor~~ housing, and an additional nimbus-pth (sensor_3) ~~is~~ was placed under the body of the UAS without a housing. This form of sensor placement facilitates an evaluation between the sensor placed inside the housing versus under the body of the UAS without housing. It also allows comparison of the ~~sensor~~ sensors mounted on the opposite ends of the UAS. Having secondary sensors also provides a fail-safe when the primary sensors fail~~-~~, such as the case on XQ2 humidity sensors on 17 July ~~,~~2018 data.

The UAS's total payload during the experiments ~~were ~kg. Sensor housing with~~ was approximately 1.8 kg. Two sensor housings with their support structure and sensor ~~is 2× ~gm, onboard computer is 140gm,~~ were approximately 720 g each; the onboard computer was 140 g; and misc cables, screws~~etc. are approx. 200gm.~~, etc., were approximately 200 g. UAS flight endurance was ~~20–25 min~~ $20 - -25$ min with the payload.

3 Flight locations ~~,~~ and strategies

3.1 Flight locations

During the LAPSE-RATE field campaign, measurement objectives for each day were determined based on the weather forecast, site availability, and available team resources. Many designated locations of San Luis Valley of Colorado, USA, were planned beforehand as atmospheric sampling sites depending on atmospheric phenomena of interest. The planning of locations, atmospheric phenomenon to be observed for the day, and assignment of teams are described in (de Boer et al., 2020a). We conducted flights

Table 2. Latitude, longitude, and mean sea level (MSL) altitude of operation locations in World Geodetic System 84 (WGS 84) decimal degrees.

Location	Latitude	Longitude	Altitude (MSL)
Golf	37.626963	-105.820028	~~2298 m~~2298 m
Gamma	37.893536	-105.716137	~~2329 m~~2329 m
Leach Airfield	37.784560	-106.044552	~~2316 m~~2316 m
India	38.051294	-106.102885	~~2332 m~~2332 m
Charlie	38.052690	-106.087414	~~2329 m~~ 2329 m

in locations designated as Golf, Gamma, Leach, India, ~~Charlie in~~ and Charlie between 14 – 19 July as part of the LAPSE-RATE flight campaign (de Boer et al., 2020b) as well as individual research objectives. GPS coordinates of ~~the~~ these locations are provided in Table 2 and illustrated in a terrain map in Figure 2. The 'inset (B)' of Figure 2 shows the flight locations of UNL UASs in the context of all the LAPSE-RATE flight campaign locations of interest where all the teams were operating based on the measurement objective of the day.

3.2 Flight strategies

Flight strategies for each day were dictated by atmospheric phenomena being measured. The teams participating in the LAPSE-RATE campaign coordinated flights across the San Luis Valley according to the atmospheric phenomena of interest for the day and the atmospheric variability expected at different sampling locations. Measurement objectives of LAPSE-RATE in which UNL participated in data collection are calibration flight (CLF), boundary layer transition (BLT), convection initiation (CI), cold air drainage flow (CDF). Table 3 shows the ~~distribution~~ locations of UASs deployed by UNL by date~~and time~~and , time, and the corresponding mission objectives.

~~On July~~ All the flights were conducted under the command of one remote pilot in command (PIC) with 'Federal Aviation Administration (FAA) part 107' license in accordance with FAA's rule. All the flights included in the dataset were conducted using preprogrammed missions in DJI Ground Station (GS) Pro app (DJI, 2021a) by the remote pilot in command (PIC), with very few exceptions of manual flights. Occasionally the remote PIC took control over segments of flight from the automatic mission control of the app when deemed safer by the PIC, e.g., passing through a turbulent layer of atmosphere. Although visual observers (VO) were not required by FAA, two VO were present at each flight location for greater situational awareness and safety during each flight. VOs were monitoring the UAS's movement, took handwritten notes about flight events and weather, and scanned the surrounding area for manned and unmanned flights.

All the flights were legally conducted under FAA Certificate of Authorization (COA) for altitudes up to 914.4 m AGL when notices to airmen (NOTAMs) were active in the blue area marked in the 'inset (A)' of Figure 2. For all our flights, however, we were limited to flying up to a 500 m maximum altitude due to the altitude limitation set in the firmware of the UAS. In the days when NOTAMs were not active for COA, all the flights were conducted up to the legal flight limit of 121 m AGL as defined in the 'part 107' regulations.

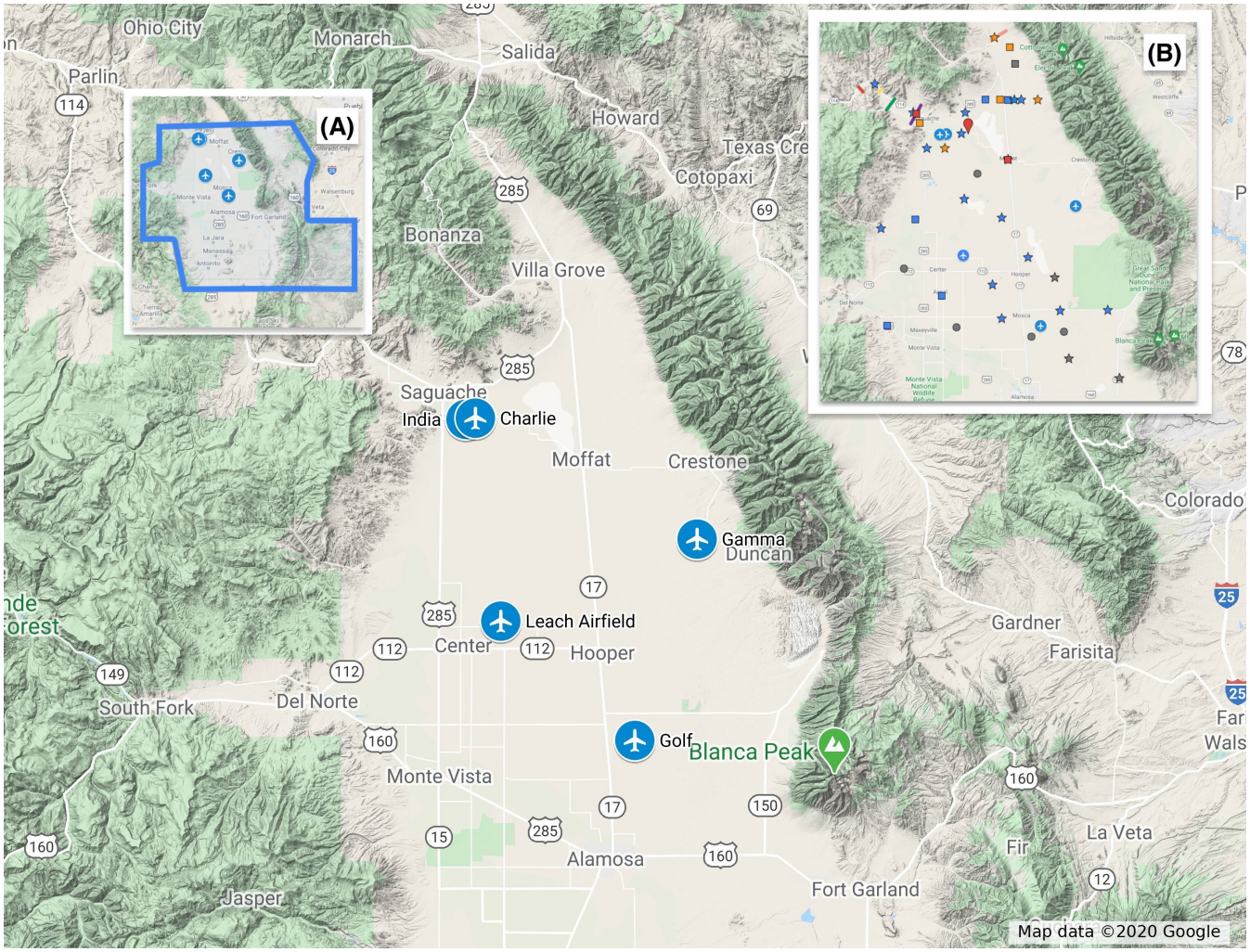

Figure 2. Flight locations of UNL UASs overlaid on the terrain map. Inset (A) shows the blue overlay area where operation of small UASs for flight altitudes up to 914.4 m AGL was authorized by the Federal Aviation Authority (FAA) Certificate of Authorization (COA) between 13 – 22 July. Inset (B) shows the spatial distribution of flight locations used by UNL and all other teams participating in the LAPSE-RATE campaign for various missions between 14 – 19 July 2018. Map data © Google 2020

Table 3. UAS locations and mission objectives for the day. Mission objectives are: Calibration flight (CLF), Boundary layer transition (BLT), Convection initiation (CI), Cold air drainage flow (CDF)

Date and Time	Objective	No. of Flight Flights	Max. Maximum Altitude	Location			
				Golf	Gamma	Leach	India
July 14 , July 2018 (17:17-17:33 MDT)	CLF	2	120 m			M600P2, M600P1 & M600P2	
July 15 , July 2018 (9:00-15:15 MDT)	CI	19	500 m	M600P2 M600P1	M600P2		
July 16 , July 2018 (8:00-14:30 MDT)	CI	47	120 m	M600P2 M600P1	M600P2		
July 17 , July 2019 (7:00-9:00 MDT)	BLT	18	100 m			M600P2, M600P1 & M600P2	
July 18 , July 2019 (7:00-14:30 MDT)	CI	43	120 m	M600P2 M600P1	M600P2		
July 19 , July 2019 (5:30-11:00 MDT)	CDF	43	500 m				M600P2 M600P1

3.2.1 14 July 2018

On 14 , July 2018, the mission objective was to compare both of the systems against a reference point, the MURC tower (?)Mobile UAS Research Collaboratory (MURC) tower (de Boer et al., 2020c), to calibrate and validate the sensor observations. MURC tower instrumentations were set to 15.2 m AGL. University of Nebraska-Lincoln (UNL) Mobile Mesonet was also collecting data about 2 m AGL for surface-level observations. Additionally, periodic radiosonde launches were conducted by National Severe Storms Laboratory (NSSL). Figure 3 shows an overview of the spatial distribution of the MURC tower, UAS platforms, and UNL Mobile Mesonet. Details about MURC tower's instrumentation, deployment strategies, and data processing can be obtained from (de Boer et al., 2020c).

One flight for each system was conducted where the UAS ascended to the height of the MURC tower (15.2 m) and hovered for 10 minutes. After that, the UAS ascended to at 120 m at 1 m s^{-1}, hovered for 30 seconds30 s, and descended at the same speed to land. This mission was performed in collaboration with all participating teams at the LAPSE-RATE campaign

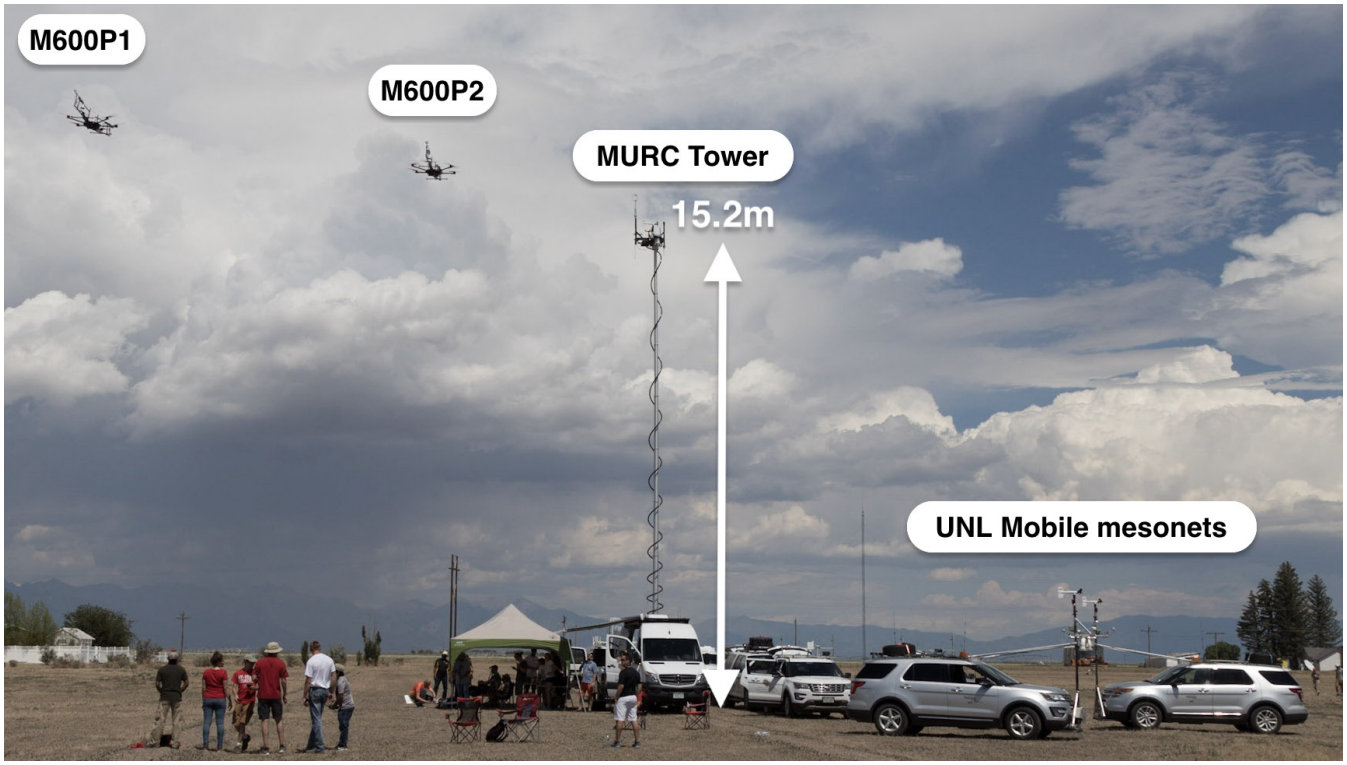

Figure 3. Coordinated data collection of the UNL UAS platforms and UNL Mobile Mesonets next to the MURC tower. UAS platforms were hovering at 15.2 m AGL (the same altitude as MURC tower instrumentation).

to provide measurement intercomparison between platforms from all teams (Barbieri et al., 2019). The data are available for the MURC tower~~and other teams are located~~ (de Boer et al., 2020c), UNL Mobile Mesonet (de Boer et al., 2020c), radiosonde (Bell et al., 2021), and all other participating teams on 14 – 15 July 2018 in the Zenodo community for LAPSE-RATE at (LAPSE-RATE Data Repository, 2021).

~~On July~~

3.2.2 15 July 2018

On 15 ~~,~~ July 2018, the mission objective of the day was convection initiation (CI). Vertical profiling flights were conducted up to ~~altitude at~~ 500 m altitude at 1 m s^{-1} ascent/descent speed ~~in~~ at the Golf and Gamma ~~location~~locations. Flights were planned to be at every 30 minutes to allow recharge of the UAS batteries while cycling through multiple sets of batteries. ~~At Golf, the~~

At the Golf location, ten flights were conducted between 8:59 – 15:14 MDT (local time). The weather was slightly cloudy in the morning ~~;~~ and clear throughout the ~~day; very~~ rest of the day. Very windy conditions existed for the last few flights. ~~At Gamma, the~~

At the Gamma location, nine flights were conducted between 9:02 – 3:15 MDT (local time). Two out of the nine data files could not be recovered due to an error in the onboard logging computer and a sensor issue. The weather was clear and windy in the morning, and slightly cloudy for the last half of the flights.

~~On July~~

3.2.3 16 July 2018

On 16 ~~,~~ July 2018, the scheduled mission objective was also CI with flights at the same locations as the previous day. Flights were limited to ~~altitude at~~ 120 m altitude at $1.5\,\mathrm{m\,s^{-1}}$ ascent/descent speed due to Notice to ~~Airman~~ Airmen (NOTAM) not being active for the day. Due to reduced altitude, more flights could be conducted with available batteries. As such, flights were conducted every 15 minutes. ~~At Golf , the~~

We performed 26 flights at Golf between 8:06 – 14:34 MDT (local time). The first two flights of the morning consisted of two consecutive profiles, but it was draining the battery a lot faster than our recharging capacity. We then switched to one profile every 15 minutes to reserve enough battery in each flight to maintain a consistent interval between profiles. The weather started slightly cloudy, and then ~~clear through out~~ remained clear throughout the day.

At Gamma, ~~the~~ 21 flights were conducted between 9:02 – 14:05 MDT (local time). All the profiles collected at this location are single profiles. The weather was clear throughout the day, with partly cloudy ~~condition for~~ conditions persisting during the last few flights.

~~On July~~

3.2.4 17 July 2018

On 17 ~~,~~ July 2018, the scheduled missions were for boundary layer transition (BLT). The ~~early morning experiments~~experiments were geared towards validation of the sensor housing by the detection of the inversion layer. We conducted the experiments in the early morning in an inversion, before sunrise, ~~help validate~~ to identify if the sensor housing ~~reading since the measurement error from the downwash~~ introduces measurement error due to the upwash or downwash of the UAS. This effect is more easily detected in stable versus well-mixed conditions ~~.~~ since air molecules from stable air airmass will maintain the temperature of the layer even when air is pushed up or down. Thus if we can verify that sensor housing detects inversion at the same level as a standard measurement (such as radiosonde), we know the readings are not affected by upwash or downwash.

We conducted simultaneous flights for both UAS with six vertical ~~profile and 3 horizontal profile~~ profiles and three horizontal profiles at various UAS movement speeds ~~. The sky was~~ between 7:00 – 8:48 MDT (local time). NSSL launched coordinated radiosonde balloons at regular intervals at the same location to be used as the ground truth measurement for UAS's data. UNL Mobile Mesonets collected measurements at 2 m AGL for surface-level observations during the entire duration of the experiments. The sky remained cloudy throughout all the flights.

~~On July~~

3.2.5 18 July 2018

On 18 ~~,~~July 2018, the scheduled mission was for CI. Flights were conducted up to ~~altitude at~~ 500 m altitude at 1.5 m s^{-1} ascent/descent speed at both Golf and Gamma locations. Flights were generally conducted every 30 minutes. ~~At the~~

At the Golf location, a total 27 of flights were performed between 7:08 – 14:20 MDT (local time). The first 17 flights were in support of the LAPSE-RATE campaign objective. At the conclusion of the day, ten additional ~~150 m~~ 150 m altitude flights were performed at ~~the Golf location at~~ various ascent/descent ~~speed~~ speeds to study the effect of UAS movement speed on temperature and humidity observations. ~~At both location,~~

At the Gamma location, 16 profile flights were conducted between 7:07 – 13:12 MDT (local time). At both locations, some flights were performed up to an altitude of 300 m, while others at 500 m.

At both locations, the sky was clear for the first half of the flights, and partly cloudy for the second half.

~~On July~~

3.2.6 19 July 2018

On 19 ~~,~~July 2018, the mission objective was cold drainage flow. UASs were placed at the Charlie and India locations for this mission. Flights were performed starting before sunrise at ~~maximum altitudes up to 350m at~~ 1.5 m s^{-1} ascent/descent speed. Flights were scheduled for every 15 minutes. Strobe lights, as per FAA regulations, were used for flights during twilight.

At the India location, 23 flights were conducted between 5:34 – 11:08 MDT (local time). Maximum flight altitudes were up to 300 m AGL for seven flights, 350 m AGL for 15 flights, 500 m AGL for one flight.

At the Charlie location, 21 flights were performed between 5:50 – 11:10 MDT (local time). Maximum flight altitudes were up to 300 m AGL for ten flights, 350 m AGL for nine flights, 500 m AGL for one flight.

At both locations, the sky was cloudy before sunrise but clear ~~afterwards~~afterward.

4 Data processing and quality control

Data are recorded from individual sensors and the UAS flight controller as they arrive ~~to the DAQ~~at the DAQ, as described earlier. The recorded data are then processed in MATLAB to synchronize using the zero-order-hold (ZOH) method to create a single output file. We used a discrete sample time of ~~1 second~~ 1 s for zero-order-hold to match the output rate of primary sensors. In the ZOH method, sample value is held constant for one sampling period, i.e., when temperature data is recorded from temperature sensors, the last known value of altitude from GPS data is recorded without any interpolation. Since the GPS data is recorded at a higher frequency from the flight controller, it is assumed to be close and within GPS's uncertainty of measurement. Invalid or missing data are replaced with -9999.9 wherever the sensor data are unavailable to the DAQ. No other processing was done on the data, such as sensor response correction, bias correction, etc.

We note that the humidity ~~sensor of the XQ2~~ observations of the primary sensor on some flights for ~~July~~ 17 ~~,~~July 2018 ~~was~~ were saturated at 100% in one of the UAS (M600P1)~~and ~~, and the corresponding data are not usable~~; ~~secondary~~ . Secondary

sensor measurements should be used to replace these data. Also, humidity readings from nimbus-pth have sensitivity issues; although it displays a similar trend as the other sensors, it does not capture the whole range of observation and will need further calibration.

~~No other processing was done on the data such as sensor response correction, bias correction, etc.File naming convention and explanation of the data fields can be found~~ Files were formatted in NetCDF format, with common variables names and meta-data added, to be consistent with all the entities collecting data for the LAPSE-RATE field campaign. A detailed explanation of the naming conventions and meta-data that were requested can be obtained from (de Boer et al., 2020b). An example file name produced by UAS platforms M600P1, and M600P2 for the data collected starting at 23:16:33 UTC on 14 July 2018 would be UNL.MR6P1.a0.20180714.231633.nc, and UNL.MR6P2.a0.20180714.231633.nc respectively. Here,

- 'UNL' is the identifier for the data collecting institution, UNL
- 'MR6P1', and 'MR6P2' are the platform identifiers for M600P1, and M600P2 respectively
- 'a0' indicates raw data converted to NetCDF
- '20180714' is UTC file date in yyyymmdd(year, month, day) format
- '231633' is UTC file start time in hhmmss(hours, minutes, seconds) format
- 'nc' is the NetCDF file extension

All the files also contain metadata for each variable with an explanation of physical measurement units, time synchronization method, sensors used for the measurement. File naming conventions and explanations are also described in the read-me file of the Zenodo data repository.

5 Special topics of interest

The following are special topics of interest that can be studied from the dataset. Our analysis that focused on these topics can be found in our previous work (Islam et al., 2019).

~~**Calibration:**~~

5.1 Calibration

Data from ~~July~~ 14 ~~,~~ July 2018 can be used with MURC data available at ~~Zenodo to obtain reference for calibration (de Boer, Gijs et al., 2020~~ the Zenodo data repository (de Boer et al., 2020c) to obtain a for calibration. Correction of bias in sensor readings during post-processing requires calibration against a known reliable measurement. It also serves as additional validation for the sensor platforms and their collected data. It also facilitates the comparison of data collected by different platforms by providing a "ground-truth" to compare against. Our previous paper (Islam et al., 2019) discusses the deviation of our observations with

MURC data over a period of 10 minutes. Other work (Barbieri et al., 2019) compares all the different ~~participating platforms~~ platforms participating in the LAPSE-RATE campaign along with ours against MURC tower data~~as well~~.

~~**Effect of ascent/descent speed:**~~

5.2 Effect of ascent/descent speed

~~To study the effect of ascent/descent speed on the sensor readings, 10 flights from M600P2 platform on July~~ Ten flights from the M600P1 platform on 18 ~~,~~July 2020 starting at 20:21 UTC (local time 14:21 MDT) can be used to study the effect of ascent/descent speed on the sensor readings. Flights were conducted up to ~~150m~~ a 150 m altitude with speeds ranging from ~~1–5m/s~~ $1-5\,\mathrm{m\,s^{-1}}$ ascent speed, and ~~1–3m/s~~ $1-3\,\mathrm{m\,s^{-1}}$ descent speed. ~~Our analysis on~~ While it is desirable to move at a faster speed to optimize battery power usage to profile at greater altitudes, it may contribute to the effective sensor response time. Characterizing the sensor response at the different ascent and descent speeds would allow for the corresponding correction in the post-processing of the data. Our analysis of these data can also be found in our paper (Islam et al., 2019).

~~**Detection of Inversion:**~~

~~To study the sensor performance within an inversion layer, the first six flight~~

5.3 Detection of Inversion

The first six flights from each platform can be used from ~~July~~ 17 ~~, 2020.~~ July 2020 to study the sensor performance within an inversion layer. The speed of flight through the inversion layer ranged from ~~0.5-5m/s~~ $0.5-5\,\mathrm{m\,s^{-1}}$ for ascent, and ~~0.5-3m/s~~ $0.5-3\,\mathrm{m\,s^{-1}}$ for descent. The flights were coordinated with radiosonde launches from National Severe Storms Laboratory (NSSL) to compare the UAS profiles against the radiosonde profiles. University of Nebraska-Lincoln (UNL) Mobile Mesonet was also collecting data at the ground for surface-level observations. Dataset for radiosonde observations by NSSL (Bell et al., 2021), and surface observations by UNL Mobile Mesonet (de Boer et al., 2020c) is uploaded to Zenodo for intercomparison. The ability to detect the inversion at the correct altitude by the UAS sensor proves that UAS is collecting the observations at the sensor level rather than from the upwash or downwash of the UAS. Additionally, detection of inversion provides confidence in the quality of the data from the sensor housing in both ascent and descent. Different ascent descent speeds are used to identify the maximum speed that can be used while still acquiring quality data. Characterization of the sensor in the inversion layer provides a means for correction of observation level in case an offset is detected in the inversion layer when compared to a radiosonde. These data could also be used for comparison to the theoretical work ~~of~~for ascent and descent rate of sensing platforms (Houston and Keeler, 2020).

~~Effect of body-relative wind direction / Horizontal transect:~~

5.4 Effect of body-relative wind direction and Horizontal transect

Data are available to study sensor performance during horizontal transect with different orientations relative to the wind. The last three flights from each platform on ~~July~~ 17 ~~,~~ July 2020 can be used for this purpose. Horizontal flight speed ranged from ~~2-10m~~$2 - 10\,\mathrm{m\,s^{-1}}$. These data can also be compared with radiosonde profile (Bell et al., 2021) and surface observations (de Boer et al., 20 to Section 5.3. The horizontal flights at different speeds against various orientations of wind provide additional characterizations for the quality of sensor data at various atmospheric wind conditions. Different horizontal flight speed simulates different incident wind speed at the sensor housing inlet and their effect on the observations. At the same time, the orientation of sensor housing simulates incident wind at different orientations and their effects on the sensor observations. The orientation characterization is particularly important as waste heat from UAS can be carried into the sensor housing in an unfavorable wind orientation. Any bias that may appear in these tests would need to be considered in the profiling flight plan to optimize the orientation of the sensor housing inlet relative to the wind to collect quality data and make appropriate corrections in the post-processing. Our analysis of these data can also be found in our previous work (Islam et al., 2019). Although traditionally multirotor UAS is used for vertical profiling; our data shows reliable data collection is also possible for horizontal profile/~~s~~transect using our sensor housing.

6 Examples of collected profile

Figure 4 shows examples of temperature and humidity profiles collected using the M600P1 platform's primary sensor. The top two panels illustrate a 500m profile taken through a well-mixed atmosphere. The bottom two panels in Figure 4 are an example of a profile taken before sunrise through a nocturnal inversion. Although the housing is designed to address ascent/descent differences, the sensor and the housing have an inherent response time that can not be eliminated. The utility of the presented sensor housing is to keep the effective response time consistent irrespective of the atmospheric condition or orientation of the sensor relative to the wind/sun. The data presented in the figures are not filtered or corrected for effective sensor response time. The raw data without any sensor response correction is presented to show the impact of proper sensor housing on the observations collected by temperature and humidity sensors. This response lag causes a deviation in ascent/descent reading as is expected. Ascent/descent deviation for humidity sensor is larger due to its slower response time in colder temperatures. Even without any correction, ascent and descent readings in our data were within the bounds of sensors uncertainty ($\pm\,0.3\,^{\circ}\mathrm{C}$ and $\pm\,5\,\%\,\mathrm{RH}$ for temperature and humidity sensors, respectively) and show how effective sensor housing is in collecting quality data. It should be noted that correction can be done using sensor response time as listed by the manufacturer in Table 1. A rigorous correction would require the characterization of the sensor installed in the housing 'as flown' (McCarthy, 1973). The data from MURC (de Boer et al., 2020c) and UNL Mobile Mesonet (de Boer et al., 2020c) can be used as an additional calibration point, as discussed in Section 5.

~~Figure~~

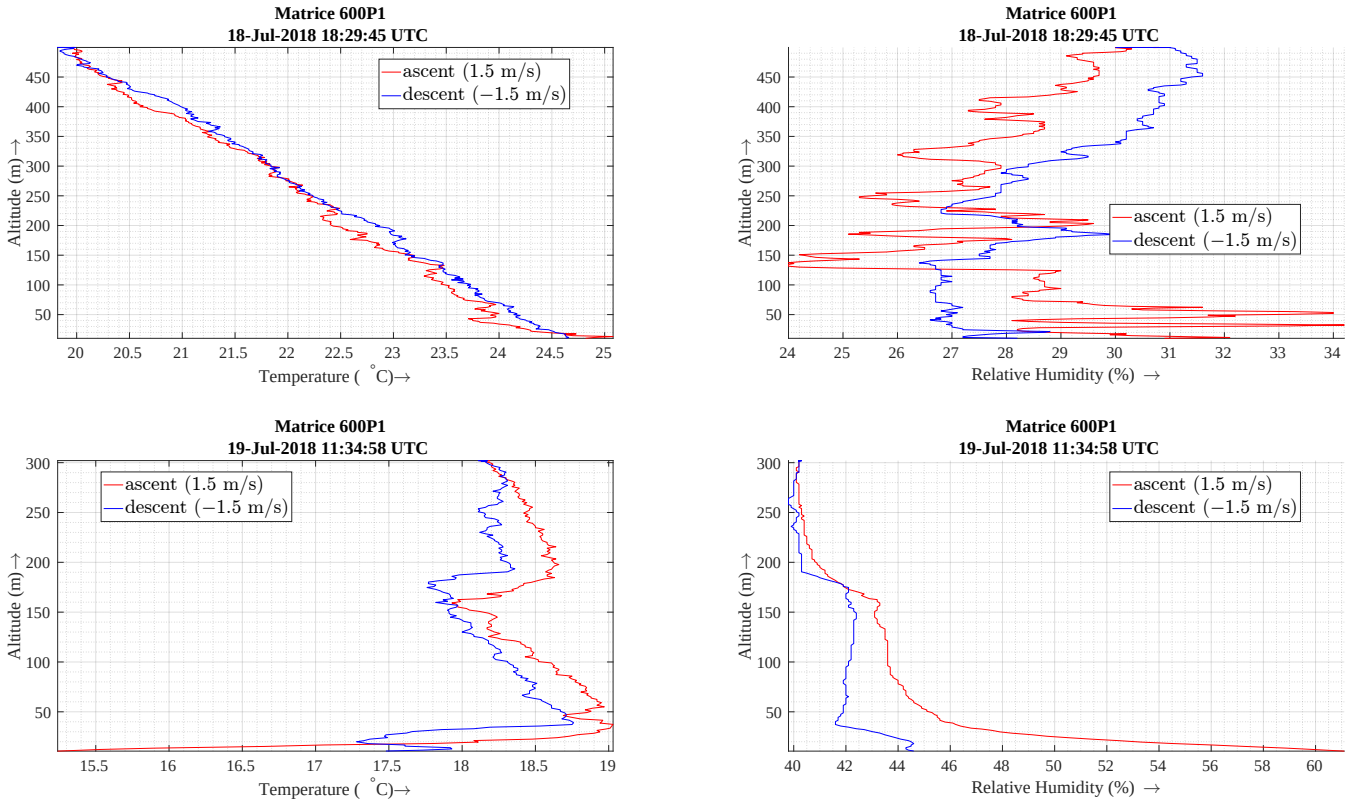

Figure 4. Examples of two vertical profiles collected using UAS: M600P1. The top row corresponds to a 500 m profile in a well-mixed atmosphere; the bottom row corresponds to a 300 m profile during a nocturnal inversion before sunrise. The figures show raw data as it was collected, thus show a difference in ascent and descent measurement as expected due to sensor response time. Humidity sensor response time is slower than temperature sensor (at the temperatures when flights were conducted), and response time changes with temperature (see Table 1). As such, the difference between ascent and descent is much larger for humidity readings, with additional variability introduced by changing sensor response time. Even without correction, it should be noted that the ascent and descent readings are within the bounds of sensors uncertainty ($\pm 0.3\,^{\circ}\mathrm{C}$ and $\pm 5\,\%\,\mathrm{RH}$ for temperature and humidity sensors, respectively) and shows how effective sensor housing is in collecting quality data.

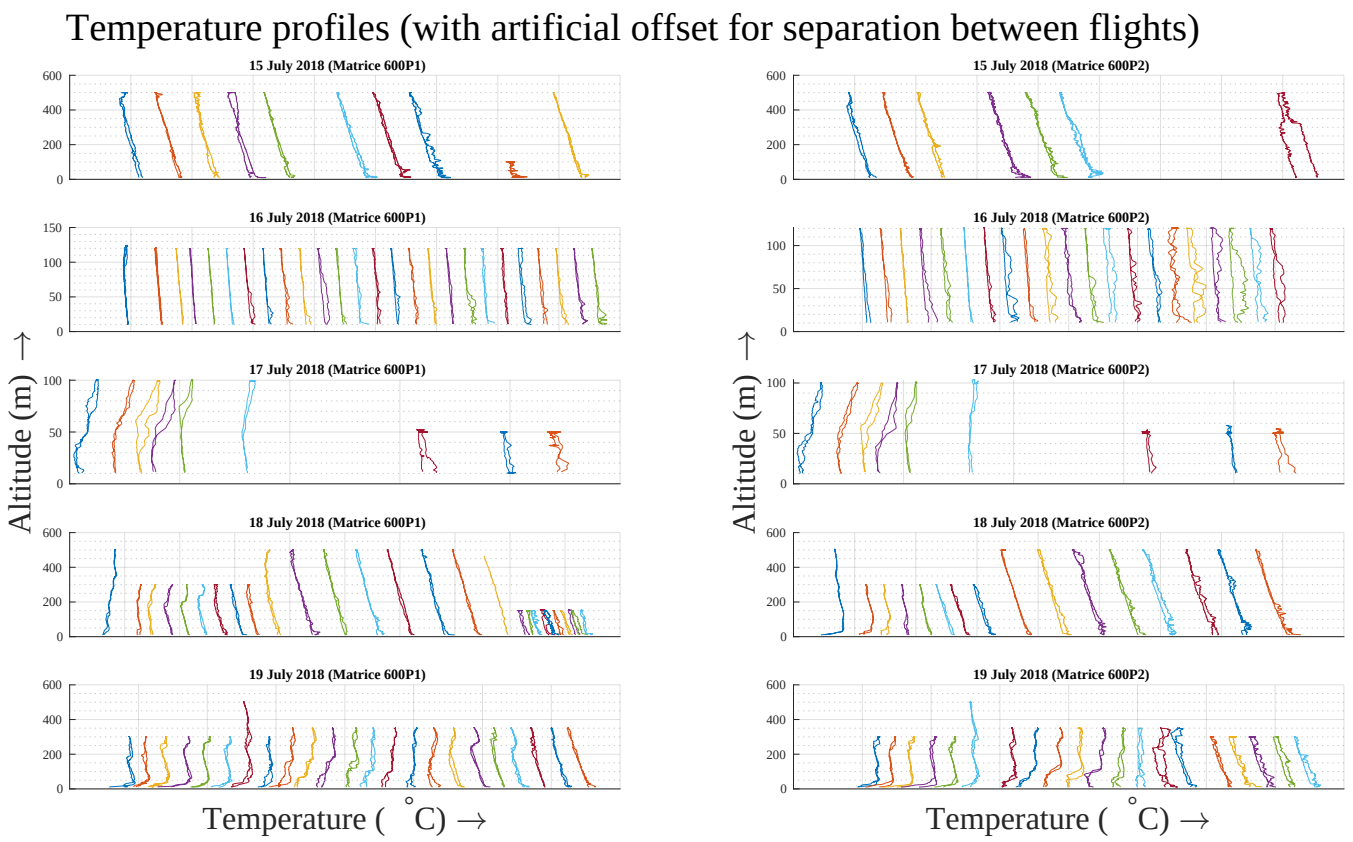

Figure 5. Temperature ~~profile~~ profiles from the primary sensor (XQ2) in all flights from ~~15-19~~ 15–19 July ~~, 2018~~2018. The horizontal axis does *not* represent a continuous temperature scale; each profile within a day is displaced along the horizontal to avoid overlap. Order from left to right on each subplot indicates the order in which flights were conducted. Table 3 can be consulted for information about flight start times and site location for each UAS on a particular day.

Figures 5 and~~Figure 6 shows~~ 6 show primary sensor (XQ2) temperature and relative humidity profiles, respectively, for all the flights conducted between ~~15-19 July ,~~ 15–19 July 2018. The profiles are plotted using ~~artificial~~ an artificial horizontal axis offset for clarity. These figures ~~serves~~ serve the purpose of a quick glance over the entire dataset and to locate interesting flights for further study. It should be noted that all the presented data are raw data as collected by the sensors without any correction for sensor response time or bias correction.

~~Examples of vertical profile collected using UAS: M600P1~~

In Figure 5, flights conducted on 15, 16, and 18 July to investigate 'Convection initiation (CI)' show a well-mixed atmosphere profile for most flights with a steady lapse rate of temperature. Data from M600P1 on 18 July at the Golf location (see Table 2 and 3) show the presence of an inversion in the early morning flights. Also, notice the last ten profiles for M600P1 with varying speed produces an ascent-descent difference of various amounts due to change in effective sensor response time. Data collected

at Leach airport to investigate 'Boundary layer transition (BLT)' on 17 July show a strong presence of an inversion in all flights. Data from 19 July collected to investigate 'Cold air drainage flow (CDF)' show progression of the ABL from inversion before sunrise in the early flights to well-mixed condition for the last few flights of the day.

In Figure 6, flights conducted on 17 July by M600P1 show primary humidity sensor failure. However, data files include secondary sensor humidity measurements that should be used for analysis instead. Since the humidity sensors have a higher sensor response time in the temperature we conducted most of our flights, it may show hysteresis higher than the temperature. We also found that the humidity sensor would collect micro dust particles as it was being flown, which could affect the accuracy of the sensors further. Another interesting feature of the humidity data presented here shows that readings are much smoother when collecting data in an inversion compared to data in a well-mixed atmosphere. Additionally, the difference between ascent and descent is much higher near ground level for most flights; this is the result of a rapid change of humidity near ground and sensor response time of humidity sensors.

7 Conclusions

As part of the LAPSE-RATE measurement campaign in July 2018 in San Luis Valley, Colorado, USA, UNL participated in data collection in support of science missions focused on convection initiation, boundary layer transition, and cold air drainage flow. UNL deployed ~~UASs in two location simultaneously for each mission~~two UASs in five locations for these missions. A total of 172 flights were conducted up to a maximum $500\,\mathrm{m}$ altitude above ground level (AGL)~~. All data are available for open access at Zenodo data repository (Islam et al., 2020).~~ , resulting in an interesting and diverse dataset that can be studied individually or along with data from other teams participating in the LAPSE-RATE campaign.

8 Data availability

Dataset is available at Zenodo with Creative commons license. https://doi.org/10.5281/zenodo.4306086 (Islam et al., 2020).

Author contributions. AH, and CD planned the contribution of the University of Nebraska-Lincoln contributions to LAPSE-RATE. AI designed the sensor housing and support structures. All authors contributed to data collection and analysis. AI, AS, and CD were part of the multirotor flight team. AI and AS contributed to data processing and presentation. AI constructed the manuscript. All authors contributed to manuscript edits. AH, and CD acquired the funding for the paper.

Competing interests. The authors declare no competing interests. The funders had no role in the design of the study; in the collection, analyses, or interpretation of the data; in the writing of the manuscript; or in the decision to publish the results.

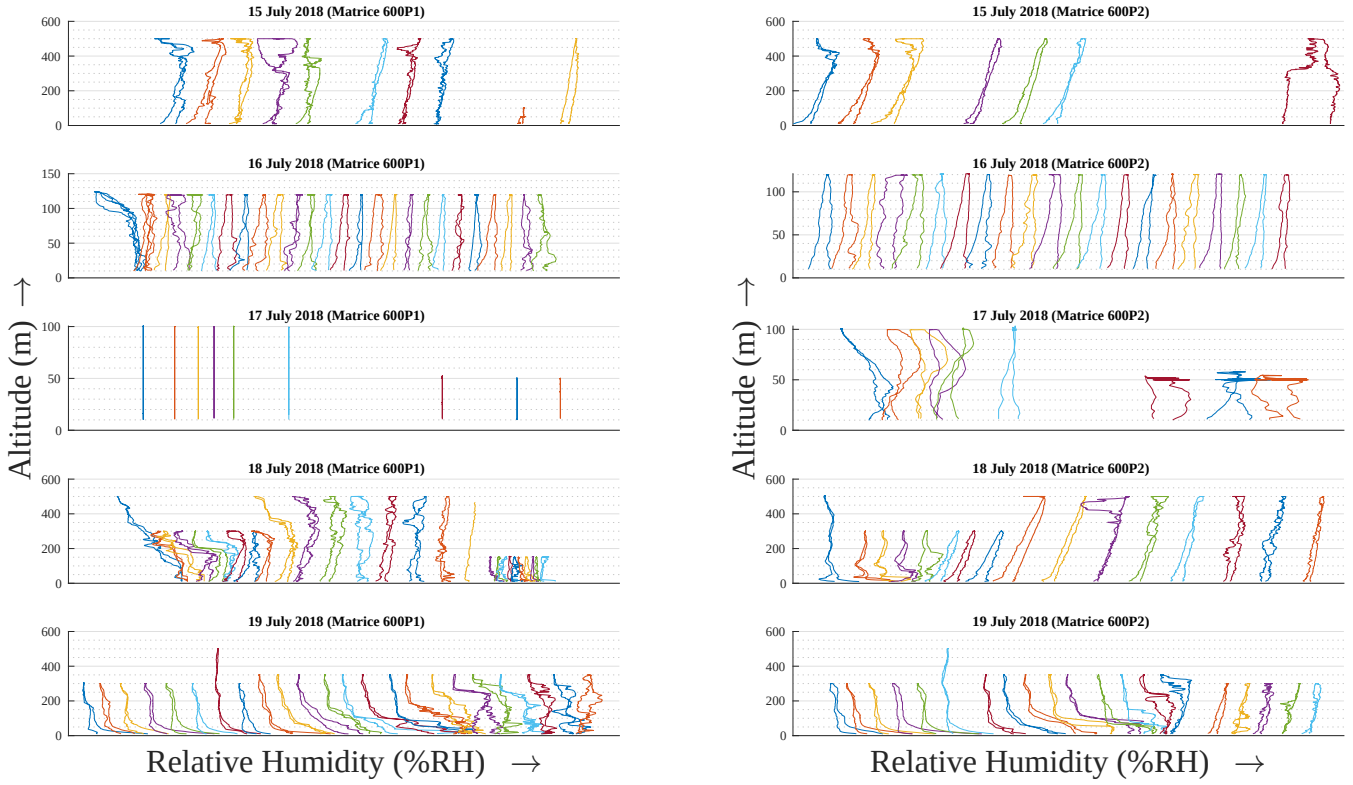

Figure 6. Relative humidity profile from the primary sensor (XQ2) in all flights from ~~15–19~~ 15–19 July ~~, 2018~~2018. The horizontal axis does *not* represent a continuous humidity scale; each profile within a day is displaced along the horizontal to avoid overlap. Order from left to right on each subplot indicates the order in which flights were conducted. Table 3 can be consulted for information about flight start times and site location for each UAS on a particular day.

Disclaimer. The views, findings, conclusions, and recommendations expressed in the manuscript are those of the authors and do not necessarily represent the views of the funding agencies.

Acknowledgements. This work was partially supported by NSF IIA-1539070, IIS-1638099, IIS-1925052, IIS-1925368, NASA ULI-80NSSC20M0162, and USDA-NIFA 2017-67021-25924. Limited general support for LAPSE-RATE was provided by the US National Science Foundation (AGS 1807199) and the US Department of Energy (DE-SC0018985) in the form of travel support for ~~early career~~ early-career participants. Support for the planning and execution of the campaign was provided by the NOAA Physical Sciences Division and NOAA UAS Program.

We thank Jason Finnegan and Amy Guo for their help with data collection during the LAPSE-RATE flight campaign. We would like to thank Dr. Sean Waugh and the National Severe Storms Laboratory for the radiosonde data. We also thank S. Borenstein and C. Dixon for their help with the MURC operations.

Islam, A., Houston, A., Shankar, A., and Detweiler, C.: University of Nebraska-Lincoln Unmanned Aerial System observations from LAPSE-RATE (Version v1) Data set, Zenodo, http://doi.org/10.5281/zenodo.4306086, 2020.

Islam, A., Houston, A.L., Shankar, A. and Detweiler, C.,: Design and evaluation of sensor housing for boundary layer profiling using multirotors, Sensors, 19(11), p.2481, https://doi.org/10.3390/s19112481, 2019.

Elston, J., Argrow, B., Stachura, M., Weibel, D., Lawrence, D., and Pope, D.: Overview of small fixed-wing unmanned aircraft for meteorological sampling, J. Atmos. Ocean. Technol., 32, 97–115, https://doi.org/10.1175/JTECH-D-13-00236.1, 2015.

Bonin, T., Chilson, P., Zielke, B., and Fedorovich, E.: Observations of the early evening boundary-layer transition using a small unmanned aerial system, Bound. Layer Meteorol., 146, 119–132, https://doi.org/10.1007/s10546-012-9760-3, 2013.

Houston, A.L., Argrow, B., Elston, J., Lahowetz, J., Frew, E.W., and Kennedy, P.C.: The collaborative Colorado–Nebraska unmanned aircraft system experiment, Bull. Am. Meteorol. Soc., 93, 39–54, https://doi.org/10.1175/2011BAMS3073.1, 2012.

Jacob, J., Chilson, P., Houston, A., and Smith, S.: Considerations for atmospheric measurements with small unmanned aircraft systems, Atmosphere, 9, 252, https://doi.org/10.3390/atmos9070252, 2018.

Houston, A., Chilson, P., Islam, A., Shankar, A., Greene, B., Segales, A., and Detweiler, C.: PTH Sensor Siting on Rotary-Wing UAS, in: Proceedings of the 19th AMS Symposium on Meteorological Observation and Instrumentation, Austin, TX, USA, 7–11 January 2018, 6.7, 2018.

DJI Matrice 600 Pro: , last access: 16 December 2020.

Odroid XU4: , last access: 16 December 2020.

Robot Operating System (ROS): , last access: 16 December 2020.

Mobile UAS Research Collaboratory (MURC): last access: 16 December 2020.

Barbieri, L., Kral, S.T., Bailey, S.C.C., Frazier, A.E., Jacob, J.D., Reuder, J., Brus, D., Chilson, P.B., Crick, C., Detweiler, C., Doddi, A., Elston, J., Foroutan, H., González-Rocha, J., Greene, B.R., Guzman, M.I., Houston, A.L., Islam, A., Kemppinen, O., Lawrence, D., Pillar-Little, E.A., Ross, S.D., Sama, M.P., Schmale, D.G., Schuyler, T.J., Shankar, A., Smith, S.W., Waugh, S., Dixon, C., Borenstein, S., and de Boer, G.: Intercomparison of Small Unmanned Aircraft System (sUAS) Measurements for Atmospheric Science during the LAPSE-RATE Campaign, Sensors, 19, 2179, https://doi.org/10.3390/s19092179, 2019.

Lower Atmospheric Profiling Studies at Elevation - a Remotely-piloted Aircraft Team Experiment (LAPSE-RATE): , last access: 16 December 2020.

de Boer, G., Borenstein, S., Dixon, C., and Argrow, B.: University of Colorado MURC Observations from LAPSE-RATE (Version 2) Data set, Zenodo, http://doi.org/10.5281/zenodo.3875493, 2020.

de Boer, G., Waugh, S., Erwin, A., Borenstein, S., Dixon, C., Shanti, W., Houston, A., and Argrow, B.: Measurements from mobile surface vehicles during LAPSE-RATE, Earth Syst. Sci. Data Discuss., https://doi.org/10.5194/essd-2020-173, in review, 2020.

Houston, A. L., and Keeler, J. M.: Sounding Characteristics that Yield Significant Convective Inhibition Errors due to Ascent Rate and Sensor Response of In Situ Profiling Systems, J. Atmos. Oceanic Technol., 37, 1163–1172, https://doi.org/10.1175/JTECH-D-19-0 2020.

Villa, T.F., Salimi, F., Morton, K., Morawska, L., and Gonzalez, F.: Development and validation of a UAV based system for air pollution measurements, Sensors, 16, 2202, https://doi.org/10.3390/s16122202, 2016.

Prudden, S., Fisher, A., Mohamed, A., and Watkins, S.: A flying anemometer quadrotor: Part 1, in: Proceedings of the International Micro Air Vehicle Conference (IMAV 2016), Beijing, China, 17–21 October 2016, 17–21, 2016.

Greene, B.R., Segales, A.R., Waugh, S., Duthoit, S., and Chilson, P.B.: Considerations for temperature sensor placement on rotary-wing unmanned aircraft systems, Atmos. Meas. Tech., 11, 5519–5530, https://doi.org/10.5194/amt-11-5519-2018, 2018.

Houston, A.L., and Keeler, J.M.: The impact of sensor response and airspeed on the representation of the convective boundary layer and airmass boundaries by small unmanned aircraft systems, J. Atmos. Ocean. Technol., 35, 1687–1699, https://doi.org/10.1175/JTECH-D-18-0019.1, 2018.

Ventura Diaz, P., and Yoon, S.: High-fidelity computational aerodynamics of multi-rotor unmanned aerial vehicles, in: Proceedings of the 2018 AIAA Aerospace Sciences Meeting, Kissimmee, FL, USA, 8–12 January 2018, p. 1266, 2018.

Yoon, S., Ventura Diaz, P., Boyd, D.D., Chan, W.M., and Theodore, C.R.: Computational aerodynamic modeling of small quadcopter vehicles, in: Proceedings of the 73rd Annual AHS International Forum and Technology Display 2017, Fort Worth, TX, USA, 9–11 May 2017, 2017.

iMet-XQ2 UAV Sensor: , last access: 2 December 2020.

iMet-XQ1 UAV Sensor: , last access: 2 December 2020.

nimbus-pth Temperature-Humidity sensor: Temperature sensor data sheet, , last access: 4 December 2020. Humidity sensor data sheet, , last access: 4 December 2020.

References

Anderson, S. P. and Baumgartner, M. F.: Radiative Heating Errors in Naturally Ventilated Air Temperature Measurements Made from Buoys*, Journal of Atmospheric and Oceanic Technology, 15, 157–173, https://doi.org/10.1175/1520-0426(1998)015<0157:rheinv>2.0.co;2, 1998.

Barbieri, L., Kral, S., Bailey, S., Frazier, A., Jacob, J., Reuder, J., Brus, D., Chilson, P., Crick, C., Detweiler, C., Doddi, A., Elston, J., Foroutan, H., González-Rocha, J., Greene, B., Guzman, M., Houston, A., Islam, A., Kemppinen, O., Lawrence, D., Pillar-Little, E., Ross, S., Sama, M., Schmale, D., Schuyler, T., Shankar, A., Smith, S., Waugh, S., Dixon, C., Borenstein, S., and de Boer, G.: Intercomparison of Small Unmanned Aircraft System (sUAS) Measurements for Atmospheric Science during the LAPSE-RATE Campaign, Sensors, 19, 2179, https://doi.org/10.3390/s19092179, 2019.

Bell, T. M., Klein, P. M., Lundquist, J. K., and Waugh, S.: Remote-sensing and radiosonde datasets collected in the San Luis Valley during the LAPSE-RATE campaign, Earth System Science Data, 13, 1041–1051, https://doi.org/10.5194/essd-13-1041-2021, 2021.

Bonin, T., Chilson, P., Zielke, B., and Fedorovich, E.: Observations of the Early Evening Boundary-Layer Transition Using a Small Unmanned Aerial System, Boundary-Layer Meteorology, 146, 119–132, https://doi.org/10.1007/s10546-012-9760-3, 2013.

Dabberdt, W. F., Schlatter, T. W., Carr, F. H., Joe Friday, E. W., Jorgensen, D., Koch, S., Pirone, M., Ralph, F. M., Sun, J., Welsh, P., Wilson, J. W., and Zou, X.: Multifunctional Mesoscale Observing Networks, Bulletin of the American Meteorological Society, 86, 961–982, https://doi.org/10.1175/bams-86-7-961, 2005.

de Boer, G., Diehl, C., Jacob, J., Houston, A., Smith, S. W., Chilson, P., Schmale, D. G., Intrieri, J., Pinto, J., Elston, J., Brus, D., Kemppinen, O., Clark, A., Lawrence, D., Bailey, S. C. C., Sama, M. P., Frazier, A., Crick, C., Natalie, V., Pillar-Little, E., Klein, P., Waugh, S., Lundquist, J. K., Barbieri, L., Kral, S. T., Jensen, A. A., Dixon, C., Borenstein, S., Hesselius, D., Human, K., Hall, P., Argrow, B., Thornberry, T., Wright, R., and Kelly, J. T.: Development of Community, Capabilities, and Understanding through Unmanned Aircraft-Based Atmospheric Research: The LAPSE-RATE Campaign, Bulletin of the American Meteorological Society, 101, E684–E699, https://doi.org/10.1175/bams-d-19-0050.1, 2020a.

de Boer, G., Houston, A., Jacob, J., Chilson, P. B., Smith, S. W., Argrow, B., Lawrence, D., Elston, J., Brus, D., Kemppinen, O., Klein, P., Lundquist, J. K., Waugh, S., Bailey, S. C. C., Frazier, A., Sama, M. P., Crick, C., Schmale III, D., Pinto, J., Pillar-Little, E. A., Natalie, V., and Jensen, A.: Data Generated during the 2018 LAPSE-RATE Campaign: An Introduction and Overview, Earth System Science Data, 12, 3357–3366, https://doi.org/10.5194/essd-12-3357-2020, 2020b.

de Boer, G., Waugh, S., Erwin, A., Borenstein, S., Dixon, C., Shanti, W., Houston, A., and Argrow, B.: Measurements from Mobile Surface Vehicles during LAPSE-RATE, Earth Syst. Sci. Data, 13, 155–169, https://doi.org/10.5194/essd-2020-173, 2020c.

de Boer, Gijs, Borenstein, S., Dixon, C., and Argrow, B.: University of Colorado MURC Observations from LAPSE-RATE, Zenodo [data set], https://doi.org/10.5281/ZENODO.3875493, 2020.

Diaz, P. V. and Yoon, S.: High-Fidelity Computational Aerodynamics of Multi-Rotor Unmanned Aerial Vehicles, in: 2018 AIAA Aerospace Sciences Meeting, p. 1266, American Institute of Aeronautics and Astronautics, Kissimmee, Florida, USA, https://doi.org/10.2514/6.2018-1266, 2018.

Digikey: Nimbus-pth Temperature Sensor Datasheet, https://media.digikey.com/pdf/Data%20Sheets/Littelfuse%20PDFs/GP103J4F.pdf, last access: 27 April 2021, 2021.

DJI: DJI Ground Station Pro, https://www.dji.com/ground-station-pro, last access: 27 April 2021, 2021a.

DJI: DJI Matrice 600 Pro - Product Information, https://www.dji.com/matrice600-pro/info, last access: 27 April 2021, 2021b.

DJI: DJI Developer - Onboard SDK, https://developer.dji.com/onboard-sdk/, last access: 27 April 2021, 2021c.

Elston, J., Argrow, B., Stachura, M., Weibel, D., Lawrence, D., and Pope, D.: Overview of Small Fixed-Wing Unmanned Aircraft for Meteorological Sampling, Journal of Atmospheric and Oceanic Technology, 32, 97–115, https://doi.org/10.1175/jtech-d-13-00236.1, 2015.

Greatwood, C., Richardson, T., Freer, J., Thomas, R., MacKenzie, A., Brownlow, R., Lowry, D., Fisher, R., and Nisbet, E.: Atmospheric Sampling on Ascension Island Using Multirotor UAVs, Sensors, 17, 1189, https://doi.org/10.3390/s17061189, 2017.

Greene, B., Segales, A., Bell, T., Pillar-Little, E., and Chilson, P.: Environmental and Sensor Integration Influences on Temperature Measurements by Rotary-Wing Unmanned Aircraft Systems, Sensors, 19, 1470, https://doi.org/10.3390/s19061470, 2019.

Greene, B. R., Segales, A. R., Waugh, S., Duthoit, S., and Chilson, P. B.: Considerations for Temperature Sensor Placement on Rotary-Wing Unmanned Aircraft Systems, Atmospheric Measurement Techniques, 11, 5519–5530, https://doi.org/10.5194/amt-11-5519-2018, 2018.

Hardkernel: ODROID-XU4, https://wiki.odroid.com/odroid-xu4/odroid-xu4, last access: 27 April 2021, 2021.

Hemingway, B., Frazier, A., Elbing, B., and Jacob, J.: Vertical Sampling Scales for Atmospheric Boundary Layer Measurements from Small Unmanned Aircraft Systems (sUAS), Atmosphere, 8, 176, https://doi.org/10.3390/atmos8090176, 2017.

Hemingway, B. L., Frazier, A. E., Elbing, B. R., and Jacob, J. D.: High-Resolution Estimation and Spatial Interpolation of Temperature Structure in the Atmospheric Boundary Layer Using a Small Unmanned Aircraft System, Boundary-Layer Meteorology, 175, 397–416, https://doi.org/10.1007/s10546-020-00512-1, 2020.

Houston, A. L. and Keeler, J. M.: The Impact of Sensor Response and Airspeed on the Representation of the Convective Boundary Layer and Airmass Boundaries by Small Unmanned Aircraft Systems, Journal of Atmospheric and Oceanic Technology, 35, 1687–1699, https://doi.org/10.1175/jtech-d-18-0019.1, 2018.

Houston, A. L. and Keeler, J. M.: Sounding Characteristics That Yield Significant Convective Inhibition Errors Due to Ascent Rate and Sensor Response of In Situ Profiling Systems, Journal of Atmospheric and Oceanic Technology, 37, 1163–1172, https://doi.org/10.1175/jtech-d-19-0191.1, 2020.

InterMet Systems: iMet-XQ1 UAV Sensor, https://www.intermetsystems.com/ee/pdf/202020_iMet-XQ_161005.pdf, last access: 27 April 2021, 2021a.

InterMet Systems: iMet-XQ2 UAV Sensor, https://www.intermetsystems.com/ee/pdf/202021_iMet-XQ2_171207.pdf, last access: 27 April 2021, 2021b.

Islam, A., Houston, A. L., Shankar, A., and Detweiler, C.: Design and Evaluation of Sensor Housing for Boundary Layer Profiling Using Multirotors, Sensors, 19, 2481, https://doi.org/10.3390/s19112481, 2019.

Islam, A., Houston, A., Shankar, A., and Detweiler, C.: University of Nebraska-Lincoln Unmanned Aerial System Observations from LAPSE-RATE, Zenodo [data set], https://doi.org/10.5281/ZENODO.4306086, 2020.

Jacob, J., Chilson, P., Houston, A., and Smith, S.: Considerations for Atmospheric Measurements with Small Unmanned Aircraft Systems, Atmosphere, 9, 252, https://doi.org/10.3390/atmos9070252, 2018.

LAPSE-RATE Data Repository: Data Repository for Lower Atmospheric Profiling Studies at Elevation - a Remotely-Piloted Aircraft Team Experiment (LAPSE-RATE), https://zenodo.org/communities/lapse-rate/?page=1&size=20, last access: 27 April 2021, 2021.

Lee, T., Buban, M., Dumas, E., and Baker, C.: On the Use of Rotary-Wing Aircraft to Sample Near-Surface Thermodynamic Fields: Results from Recent Field Campaigns, Sensors, 19, 10, https://doi.org/10.3390/s19010010, 2018.

Leuenberger, D., Haefele, A., Omanovic, N., Fengler, M., Martucci, G., Calpini, B., Fuhrer, O., and Rossa, A.: Improving High-Impact Numerical Weather Prediction with Lidar and Drone Observations, Bulletin of the American Meteorological Society, 101, E1036–E1051, https://doi.org/10.1175/bams-d-19-0119.1, 2020.

McCarthy, J.: A Method for Correcting Airborne Temperature Data for Sensor Response Time, Journal of Applied Meteorology and Climatology, 12, 211–214, https://doi.org/10.1175/1520-0450(1973)012<0211:amfcat>2.0.co;2, 1973.

Mitchell, T., Hartman, M., Johnson, D., Allamraju, R., Jacob, J. D., and Epperson, K.: Testing and Evaluation of UTM Systems in a BVLOS Environment, in: AIAA AVIATION 2020 FORUM, American Institute of Aeronautics and Astronautics, VIRTUAL EVENT, https://doi.org/10.2514/6.2020-2888, 2020.

Mouser: Nimbus-pth Humidity Sensor Datasheet, https://www.mouser.com/datasheet/2/682/Sensirion_Humidity_Sensors_SHT3x_Datasheet_digital-971521.pdf, last access: 27 April 2021, 2021.

Nolan, P., Pinto, J., González-Rocha, J., Jensen, A., Vezzi, C., Bailey, S., de Boer, G., Diehl, C., Laurence, R., Powers, C., Foroutan, H., Ross, S., and Schmale, D.: Coordinated Unmanned Aircraft System (UAS) and Ground-Based Weather Measurements to Predict Lagrangian Coherent Structures (LCSs), Sensors, 18, 4448, https://doi.org/10.3390/s18124448, 2018.

Palomaki, R. T., Rose, N. T., van den Bossche, M., Sherman, T. J., and De Wekker, S. F. J.: Wind Estimation in the Lower Atmosphere Using Multirotor Aircraft, Journal of Atmospheric and Oceanic Technology, 34, 1183–1191, https://doi.org/10.1175/jtech-d-16-0177.1, 2017.

Prudden, S., Fisher, A., Mohamed, A., and Watkins, S.: A Flying Anemometer Quadrotor: Part 1, in: Proceedings of the International Micro Air Vehicle Conference (IMAV 2016), pp. 17–21, Beijing, China, 2016.

Quigley, M., Conley, K., Gerkey, B., Faust, J., Foote, T., Leibs, J., Wheeler, R., and Ng, A. Y.: ROS: an open-source Robot Operating System, in: ICRA workshop on open source software, vol. 3, p. 5, Kobe, Japan, 2009.

ROS: Robot Operating System (ROS), https://www.ros.org/, last access: 27 April 2021, 2021.

Segales, A. R., Greene, B. R., Bell, T. M., Doyle, W., Martin, J. J., Pillar-Little, E. A., and Chilson, P. B.: The CopterSonde: An Insight into the Development of a Smart Unmanned Aircraft System for Atmospheric Boundary Layer Research, Atmospheric Measurement Techniques, 13, 2833–2848, https://doi.org/10.5194/amt-13-2833-2020, 2020.

Villa, T., Salimi, F., Morton, K., Morawska, L., and Gonzalez, F.: Development and Validation of a UAV Based System for Air Pollution Measurements, Sensors, 16, 2202, https://doi.org/10.3390/s16122202, 2016.

Yoon, S., Diaz, P. V., Jr, D. D. B., Chan, W. M., and Theodore, C. R.: Computational Aerodynamic Modeling of Small Quadcopter Vehicles, in: Yoon, Seokkwan, P. Ventura Diaz, D. Douglas Boyd Jr, William M. Chan, and Colin R. Theodore. "Computational Aerodynamic Modeling of Small Quadcopter Vehicles." In American Helicopter Society (AHS) 73rd Annual Forum, p. 16, Fort Worth, Texas, USA, 2017.